

# The surprising influence of late charged current weak interactions on Big Bang Nucleosynthesis

E. Grohs\*

*Department of Physics, University of Michigan, Ann Arbor, Michigan 48109, USA*

G.M. Fuller

*Department of Physics, University of California, San Diego, La Jolla, California 92093, USA*

---

## Abstract

The weak interaction charged current processes ( $\nu_e + n \leftrightarrow p + e^-$ ;  $\bar{\nu}_e + p \leftrightarrow n + e^+$ ;  $n \leftrightarrow p + e^- + \bar{\nu}_e$ ) interconvert neutrons and protons in the early universe and have significant influence on Big Bang Nucleosynthesis (BBN) light-element abundance yields, particularly that for  ${}^4\text{He}$ . We demonstrate that the influence of these processes is still significant even when they operate well below temperatures  $T \sim 0.7 \text{ MeV}$  usually invoked for “weak freeze-out,” and in fact down nearly into the alpha-particle formation epoch ( $T \approx 0.1 \text{ MeV}$ ). This physics is correctly captured in commonly used BBN codes, though this late-time, low-temperature persistent effect of the isospin-changing weak processes, and the sensitivity of the associated rates to lepton energy distribution functions and blocking factors are not widely appreciated. We quantify this late-time influence by analyzing weak interaction rate dependence on the neutron lifetime, lepton energy distribution functions, entropy, the proton-neutron mass difference, and Hubble expansion rate. The effects we point out here render BBN a keen probe of any beyond-standard-model physics that alters lepton number/energy distributions, even subtly, in epochs of the early universe all the way down to near  $T = 100 \text{ keV}$ .

*Keywords:* Big Bang Nucleosynthesis, Weak Interactions, Cosmological Neutrinos, Early Universe

---

## 1. Introduction

In this paper we examine individual charged current weak interactions in the Big Bang Nucleosynthesis (BBN) epoch and uncover a feature of these which is surprising and explains how BBN can be sensitive to any physics which

---

\*Corresponding author

*Email addresses:* [egrohs@umich.edu](mailto:egrohs@umich.edu) (E. Grohs), [gfuller@ucsd.edu](mailto:gfuller@ucsd.edu) (G.M. Fuller)

even slightly alters neutrino energy distribution functions, even at relatively low temperatures. The importance of this sensitivity for containing and probing beyond-standard-model (BSM) physics will be heightened as the precision of the observationally inferred primordial abundances of deuterium [1, 2] and helium [3] increases in the future.

BBN is a great success story of the marriage of nuclear and particle physics and cosmology [4, 5, 6, 7]. In essence, the light element abundances that emerge from the early universe are set in a freeze-out from nuclear statistical equilibrium (NSE). NSE is thermal and chemical equilibrium among all nuclei, where the abundance of any nuclear species is given by a Saha equation that depends only on nuclear binding energy, entropy-per-baryon, temperature, and the neutron-to-proton ratio (i.e. the ratio of neutron to proton number densities; denoted  $n/p$  ratio) [8]. NSE obtains when the rates of strong and electromagnetic nuclear reactions are fast compared to the rate at which thermodynamic conditions change, in this case governed mostly by the Hubble expansion rate. NSE freeze-out in the early universe is actually a series of freeze-outs of individual nuclear reactions and is a protracted event, taking place over many Hubble times. This endurance is a key reason why the eventual BBN light element abundance yields are sensitive to slow and relatively small, weak interaction-induced changes in the  $n/p$  ratio during the NSE freeze-out process.

The weakness of gravitation, along with an entropy-per-baryon ( $\sim 9 \times 10^9$  Boltzmann’s constant per baryon) which is large on a nuclear physics scale, and very small net electron, muon, and tau lepton numbers, combine to dictate most of what happens in NSE freeze-out. Gravitation drives the Hubble expansion, so it is inherently slow, and in the relevant radiation-dominated conditions the Hubble expansion rate is  $H \propto T^2/m_{\text{pl}}$ , where  $T$  is the plasma temperature and  $m_{\text{pl}} \simeq 1.221 \times 10^{22}$  MeV is the Planck mass. This expansion rate is so slow that at temperatures  $T > 1$  MeV, the weak interaction can maintain equilibrium by efficiently scattering and exchanging energy between the seas of neutrinos and the photon-electron-positron plasma. Typical weak interaction rates involving neutrinos and electrons/positrons are  $\sim G_F^2 T^5$ , with  $G_F \simeq 1.166 \times 10^{-11}$  MeV<sup>-2</sup> the Fermi coupling constant. The number of baryons is very small (baryon-to-photon ratio  $\eta \approx 6 \times 10^{-10}$ ) and so lepton scattering and captures on them are negligible in effecting energy transfer between the neutrino seas and the photon-electron-positron plasma. Nevertheless, the baryons and neutrino seas are in chemical equilibrium at high temperature. As the universe expands and the temperature drops, neutrinos cease to efficiently exchange energy with the plasma and, eventually, completely decouple and free fall through spacetime. Likewise, the rates of neutron-to-proton converting (i.e., isospin-changing) weak interactions decrease as the temperature drops and, eventually the  $n/p$  ratio will be dominated by neutron decay. The former decoupling process is termed “weak decoupling”, while the latter is dubbed “Weak Freeze-Out” (WFO).

The standard narrative has these as distinct events, weak decoupling at  $T \sim 1$  MeV, and WFO at  $T \sim 0.7$  MeV. This narrative is incorrect (see e.g., Refs. [9, 10, 11]).

In fact, weak decoupling and WFO are not events that are instantaneous in

time or temperature. Weak decoupling, WFO, and aspects of NSE freeze-out, all occur more or less contemporaneously over many, many Hubble times. This fact dictates the use of a numerical approach to BBN, first done by Refs. [12, 13], but it also sets up the sensitivity to late-changing weak interactions and their dependence on neutrino distribution functions which we examine in this paper.

The organization of this paper is as follows. In section 2 we give a brief exposition of the relevant charged current, isospin-changing weak interaction processes and the rates of these in the BBN epoch. In Sec. 3, we present calculations which elucidate the physics of WFO and highlight the inadequacy of neglecting *any* of the weak interactions at temperatures  $T \gtrsim 100$  keV. We give our conclusions in Sec. 4. Throughout this paper we use natural units,  $\hbar = c = k_B = 1$ , and assume neutrinos are massless at the temperature scales of interest.

## 2. The $n \leftrightarrow p$ rates

Three processes convert neutrons ( $n$ ) into protons ( $p$ ) in the BBN epoch. These are schematically shown as

$$\nu_e + n \rightarrow p + e^-, \quad (1)$$

$$e^+ + n \rightarrow p + \bar{\nu}_e, \quad (2)$$

$$n \rightarrow p + \bar{\nu}_e + e^-, \quad (3)$$

where  $e^\pm$  denote positron, electron, and  $\nu_e, \bar{\nu}_e$  denote electron neutrino, antineutrino. Additionally, the three corresponding reverse processes convert protons into neutrons

$$e^- + p \rightarrow n + \nu_e, \quad (4)$$

$$\bar{\nu}_e + p \rightarrow n + e^+, \quad (5)$$

$$\bar{\nu}_e + e^- + p \rightarrow n. \quad (6)$$

Together, the rates associated with processes (1) – (6) are the neutron-to-proton rates ( $n \leftrightarrow p$  rates). At high temperature, the rates associated with the capture processes in (1), (2), (4), and (5) are all much faster than the Hubble expansion rate. Note processes (1) – (2) have no energy threshold for lepton capture because the neutron is heavier than the proton with mass difference  $\delta m_{np} \equiv m_n - m_p \approx 1.293$  MeV. In turn, the lepton capture processes (4) – (6) have an energy threshold. As we will see below, this threshold makes a significant difference on the leverage these processes have on the  $n/p$  ratio, especially at low temperature. The three-body process (6) is not a dominant contribution. Other weak interactions on nuclei are present during BBN [14], but we focus on the  $n \leftrightarrow p$  rates for this work.

A self-consistent treatment of WFO includes calculating the  $n \leftrightarrow p$  rates within a BBN nuclear-reaction network. We use the BURST code to treat WFO self-consistently with BBN [15], although other codes also correctly capture the

physics of WFO (see Refs. [16, 17, 18]). To examine the interplay between the  $n/p$  ratio and the primordial abundances, we will modify the  $n \leftrightarrow p$  rates in BURST to employ limiting scenarios on WFO. We expect the altered scenarios to yield different results for the  $n/p$  ratio and abundances as compared to baseline computations that do not employ the said limits. Our aim will be to assess how effective each scenario is for accurately characterizing WFO and predicting primordial abundances.

To begin our analysis, we need expressions for the  $n \leftrightarrow p$  rates suitable for computational implementation. Ref. [19] gives a prescription to calculate the collision integral for the full quantum kinetic equation (QKE) for each process in (1) – (6). We do not utilize the full QKE treatment in this work (see Refs. [20, 21, 22, 23, 24, 25, 26, 27, 28, 29] for discussion on the QKEs). Instead, we employ multiple approximations to facilitate ease in numerically computing the  $n \leftrightarrow p$  rates. We start with the collision integral for the QKE in processes (1) and (4), i.e. the gain and loss terms in the reaction  $\nu_e n \leftrightarrow p e^-$ . Ref. [19] writes the collision term for the change in neutrino occupation number, i.e.  $df_{\nu_e}/dt$ . The change in the total number of neutrinos is identical to the change in the total number of neutrons, implying we can write an integrated collision term with  $n(Q_1) + \nu_e(Q_2) \leftrightarrow p(Q_3) + e^-(Q_4)$ , where  $Q_i$  is the four-momentum for particle  $i$ , for the change in the number of neutrons. The result is the following Boltzmann equation [30]

$$\begin{aligned} \left. \frac{dY_n}{dt} \right|_{\nu_e n \leftrightarrow p e^-} &= \frac{1}{n_b} \int \widetilde{dq}_1 \widetilde{dq}_2 \widetilde{dq}_3 \widetilde{dq}_4 \\ &\quad \times (2\pi)^4 \delta^{(4)}(Q_1 + Q_2 - Q_3 - Q_4) \\ &\quad \times \langle |\mathcal{M}|^2 \rangle F(E_1, E_2, E_3, E_4), \end{aligned} \quad (7)$$

where  $Y_n$  is the neutron abundance. We define abundances to be the ratio of number densities,  $Y_i \equiv n_i/n_b$ , where  $n_i$  is the number density of species  $i$  and  $n_b$  is the baryon number density. In Eq. (7), we use the phase-space notation

$$\widetilde{dq}_i \equiv \frac{d^3 q_i}{(2\pi)^3 2E_i}, \quad (8)$$

for three-momentum magnitude  $q_i$  and energy  $E_i$ .  $\delta^{(4)}(Q_1 + Q_2 - Q_3 - Q_4)$  is a four-momentum conserving Dirac delta function and  $F$  is the statistical factor appropriate for Fermi-Dirac statistics

$$\begin{aligned} F &= f_p(E_3) f_{e^-}(E_4) [1 - f_n(E_1)] [1 - f_{\nu_e}(E_2)] \\ &\quad - f_n(E_1) f_{\nu_e}(E_2) [1 - f_p(E_3)] [1 - f_{e^-}(E_4)], \end{aligned} \quad (9)$$

where  $f_i(E_i)$  is the occupation number for species  $i$  at energy  $E_i$ . We depart from the quantum description of Ref. [19] and use neutrino occupation numbers instead of the generalized density matrices for this work. For the specific

processes in Eqs. (1) and (4), the summed-squared-amplitude is [19]

$$\begin{aligned} \langle |\mathcal{M}|^2 \rangle = 2^4 G_F^2 \{ & (g_A + 1)^2 (Q_1 \cdot Q_2)(Q_3 \cdot Q_4) \\ & + (g_A - 1)^2 (Q_1 \cdot Q_4)(Q_2 \cdot Q_3) \\ & + (g_A^2 - 1) m_n m_p (Q_2 \cdot Q_4) \}, \end{aligned} \quad (10)$$

where  $g_A \simeq 1.27$  is the axial-vector coupling and  $m_n$  ( $m_p$ ) is the neutron (proton) vacuum mass. We can simplify Eq. (10), if we make the following approximations:

1. Assume the energy is much larger than the magnitude of the three momenta for the baryons.
2. Assume the mass of the baryons is approximately equal to the energy.
3. Assume the neutrino is massless, i.e.  $E_2 = q_2$ .

Under the above assumptions, Eq. (10) simplifies to:

$$\langle |\mathcal{M}|^2 \rangle = 2^4 G_F^2 E_1 E_2 E_3 E_4 \left[ 1 + 3g_A^2 + (g_A^2 - 1) \frac{q_4}{E_4} \cos \theta_{24} \right], \quad (11)$$

where  $\theta_{24}$  is the angle between  $\vec{q}_2$  and  $\vec{q}_4$ . We are free to define our coordinate system such that  $\theta_{24}$  is coincident with one of the elevation angles in either  $d^3q_2$  or  $d^3q_4$ . Therefore, the integral over the  $\cos \theta_{24}$  term in Eq. (11) will vanish, leaving a remaining nonzero portion of the summed-squared-amplitude

$$\langle |\mathcal{M}|^2 \rangle \rightarrow 2^4 G_F^2 E_1 E_2 E_3 E_4 (1 + 3g_A^2). \quad (12)$$

Eq. (12) contains no angular dependence and is straightforward to integrate in Eq. (7) with additional approximations. We use Fermi-Dirac (FD) statistics to describe the  $\nu_e$  and  $e^-$ , but simplify to Maxwell-Boltzmann (MB) statistics for the neutron and proton. This simplification allows us to make the approximation  $[1 - f_{n,p}] \approx 1$ , which in turn simplifies the statistical factor  $F$ . We relabel the second energy dummy variable,  $E_2 \rightarrow E_\nu$ , and reduce Eq. (7) to a single integration

$$\begin{aligned} \left. \frac{dY_n}{dt} \right|_{\nu_e n \leftrightarrow p e^-} = \frac{G_F^2 (1 + 3g_A^2)}{2\pi^3} \int_0^\infty dE_\nu E_\nu^2 (E_\nu + \delta m_{np}) \sqrt{(E_\nu + \delta m_{np})^2 - m_e^2} \\ \times \{ Y_p [1 - f_{\nu_e}(E_\nu)] [f_{e^-}(E_\nu + \delta m_{np})] \\ - Y_n [f_{\nu_e}(E_\nu)] [1 - f_{e^-}(E_\nu + \delta m_{np})] \}, \end{aligned} \quad (13)$$

where  $m_e$  is the electron rest mass. Eq. (13) contains two contributions: a creation component proportional to the proton abundance  $Y_p$ , deduced from process (4); and a destruction component proportional to the neutron abundance  $Y_n$ , deduced from (1). We write the creation component as

$$\left( \frac{dY_n}{dt} \right)^+ \equiv \frac{G_F^2 (1 + 3g_A^2)}{2\pi^3} Y_p T_{\text{cm}}^5 \mathcal{N}, \quad (14)$$

where we have written the integral over  $E_\nu$  as  $T_{\text{cm}}^5 \mathcal{N}$ .  $T_{\text{cm}}$  is the comoving temperature parameter and is inversely proportional to the scale factor,  $a$ , such that  $T_{\text{cm}} = T_{\text{in}}(a_{\text{in}}/a)$  where  $T_{\text{in}}$  ( $a_{\text{in}}$ ) is the plasma temperature (scale factor) taken at an initial epoch of our choosing [11]. For the purposes of studying WFO, we will set  $T_{\text{in}} = 10$  MeV.  $\mathcal{N}$  is a dimensionless number and depends on the temperature quantities through the ratios  $\delta m_{np}/T_{\text{cm}}$ ,  $m_e/T_{\text{cm}}$ , and  $T_{\text{cm}}/T$ .

We can approximate the Hubble expansion rate during radiation dominated conditions using the effective degrees of freedom statistic,  $g_\star$ , to yield [31]

$$H = \sqrt{\frac{8\pi}{3m_{\text{pl}}^2} \frac{\pi^2}{30} g_\star T_{\text{cm}}^4}, \quad (15)$$

If we equate Eq. (15) with Eq. (14), we find a comoving temperature value,  $T_{\text{eq}}$ , where the two rates are equal

$$T_{\text{eq}} \equiv \left[ \frac{2\pi^3}{m_{\text{pl}} G_F^2 (1 + 3g_A^2)} \frac{1}{Y_p \mathcal{N}} \sqrt{\frac{8\pi^3}{90} g_\star} \right]^{1/3}. \quad (16)$$

If we take  $\mathcal{N} \simeq 4!$ ,  $g_\star = 10.75$ , and  $Y_p \simeq 1$ , we calculate  $T_{\text{eq}} \simeq 0.9$  MeV in line with the nominal estimate of 0.7 MeV for WFO [see Eq. (57) in Ref. [5] and references therein]. For  $T_{\text{cm}} > T_{\text{eq}}$ , the creation term  $(dY_n/dt)^+$  is larger than the Hubble rate, and vice versa for  $T_{\text{cm}} < T_{\text{eq}}$ .

In our calculations, we assume neutrinos instantaneously decoupled from the plasma at a comoving temperature parameter  $T_{\text{cm}} > T_{\text{eq}}$ . The nucleosynthesis effects from the altered WFO scenarios dwarf the contributions from neutrino energy transport (see Refs. [9, 10, 11]). Furthermore, we do not include higher order corrections to the  $n \leftrightarrow p$  rates from finite temperature radiative corrections or modified dispersion relations of the charged leptons. See Refs. [32, 33, 34] for detailed accounting of the changes to the primordial abundances induced from these corrections. We do include Coulomb corrections from Refs. [35, 36] to processes (1), (3), (4), and (6). In addition, we include the zero-temperature radiative corrections of Refs. [32, 34] to all six processes.

In simplifying the amplitude in Eq. (12), we treated the baryons as nonrelativistic when we set  $m \sim E$ . This allowed us to separate any dependence the energy-conserving part of the four-dimensional delta function had on the nucleon energies [ $E_1$  and  $E_3$  in Eq. (7)], thereby eliminating the explicit presence of the baryon MB occupation numbers. The approximation of large baryon rest mass employed here induces a change of a few percent. See Refs. [19, 34, 37] for details on how to construct the Boltzmann equation with baryons obeying MB or FD statistics without the large baryon mass approximation. We neglect these corrections here in the spirit of exploring the leverage that weak isospin-changing interactions have during the BBN epoch. However, our conclusion that these processes are surprisingly effective at low temperature, highlight the need for including small corrections in a high-precision assessment of BBN absolute abundance yields.

Reference [19] further gives the prescription to find  $\langle |\mathcal{M}|^2 \rangle$  for the other two reactions, namely  $e^+n \leftrightarrow p\bar{\nu}_e$  and  $n \leftrightarrow p\bar{\nu}_ee^-$ . Using the same approximations in determining Eq. (12) for  $\nu_e n \leftrightarrow pe^-$ , the expressions for  $\langle |\mathcal{M}|^2 \rangle$  in the two other reactions are identical to that in (12). In order to account for the contribution of each rate to either the neutron or proton abundance change, we will write the Boltzmann equations as the following

$$\frac{dY_n}{dt} = -Y_n(\lambda_{\nu_e n} + \lambda_{e^+n} + \lambda_{n \text{ decay}}) + Y_p(\lambda_{e^-p} + \lambda_{\bar{\nu}_e p} + \lambda_{\bar{\nu}_e e^-p}), \quad (17)$$

$$\frac{dY_p}{dt} = Y_n(\lambda_{\nu_e n} + \lambda_{e^+n} + \lambda_{n \text{ decay}}) - Y_p(\lambda_{e^-p} + \lambda_{\bar{\nu}_e p} + \lambda_{\bar{\nu}_e e^-p}). \quad (18)$$

The neutron destruction (proton creation) rates are  $\lambda_{\nu_e n}$ ,  $\lambda_{e^+n}$ ,  $\lambda_{n \text{ decay}}$  and correspond to processes (1) – (3), respectively. The neutron creation (proton destruction) rates are  $\lambda_{e^-p}$ ,  $\lambda_{\bar{\nu}_e p}$ ,  $\lambda_{\bar{\nu}_e e^-p}$  and correspond to processes (4) – (6), respectively. Eqs. (17) and (18) give the changes in the neutron and proton abundances from the weak interactions. Nuclear reactions such as deuterium ( $d$ ) production in  $n(p, \gamma)d$  also affect the free neutron and proton abundances and would enter into both expressions (17) and (18). For the sake of brevity, we have ignored the nuclear contributions in writing Eqs. (17) and (18) so that we can define the weak rates  $\lambda_i$  corresponding to processes (1) – (6). In the actual numerical calculations, the nuclear reaction contributions are indispensable in Eqs. (17) and (18), and are compulsory for baryon number conservation.

We arrive at the following expressions for the six  $n \leftrightarrow p$  rates in Eqs. (17) and (18)

$$\begin{aligned} \lambda_{\nu_e n} = \frac{G_F^2(1+3g_A^2)}{2\pi^3} \int_0^\infty dE_\nu C(E_\nu + \delta m_{np}) Z(E_\nu + \delta m_{np}, E_\nu) \\ \times E_\nu^2(E_\nu + \delta m_{np}) \sqrt{(E_\nu + \delta m_{np})^2 - m_e^2} \\ \times [f_{\nu_e}(E_\nu)][1 - f_{e^-}(E_\nu + \delta m_{np})], \end{aligned} \quad (19)$$

$$\begin{aligned} \lambda_{e^+n} = \frac{G_F^2(1+3g_A^2)}{2\pi^3} \int_{\delta m_{np}+m_e}^\infty dE_\nu Z(E_\nu - \delta m_{np}, E_\nu) \\ \times E_\nu^2(E_\nu - \delta m_{np}) \sqrt{(E_\nu - \delta m_{np})^2 - m_e^2} \\ \times [1 - f_{\bar{\nu}_e}(E_\nu)][f_{e^+}(E_\nu - \delta m_{np})], \end{aligned} \quad (20)$$

$$\begin{aligned} \lambda_{n \text{ decay}} = \frac{G_F^2(1+3g_A^2)}{2\pi^3} \int_0^{\delta m_{np}-m_e} dE_\nu C(\delta m_{np} - E_\nu) Z(\delta m_{np} - E_\nu, E_\nu) \\ \times E_\nu^2(\delta m_{np} - E_\nu) \sqrt{(\delta m_{np} - E_\nu)^2 - m_e^2} \\ \times [1 - f_{\bar{\nu}_e}(E_\nu)][1 - f_{e^-}(\delta m_{np} - E_\nu)], \end{aligned} \quad (21)$$

$$\begin{aligned}
\lambda_{e^-p} = \frac{G_F^2(1+3g_A^2)}{2\pi^3} \int_0^\infty dE_\nu C(E_\nu + \delta m_{np}) Z(E_\nu + \delta m_{np}, E_\nu) \\
\times E_\nu^2(E_\nu + \delta m_{np}) \sqrt{(E_\nu + \delta m_{np})^2 - m_e^2} \\
\times [1 - f_{\nu_e}(E_\nu)] [f_{e^-}(E_\nu + \delta m_{np})], \quad (22)
\end{aligned}$$

$$\begin{aligned}
\lambda_{\bar{\nu}_e p} = \frac{G_F^2(1+3g_A^2)}{2\pi^3} \int_{\delta m_{np}+m_e}^\infty dE_\nu Z(E_\nu - \delta m_{np}, E_\nu) \\
\times E_\nu^2(E_\nu - \delta m_{np}) \sqrt{(E_\nu - \delta m_{np})^2 - m_e^2} \\
\times [f_{\bar{\nu}_e}(E_\nu)] [1 - f_{e^+}(E_\nu - \delta m_{np})], \quad (23)
\end{aligned}$$

$$\begin{aligned}
\lambda_{\bar{\nu}_e e^-p} = \frac{G_F^2(1+3g_A^2)}{2\pi^3} \int_0^{\delta m_{np}-m_e} dE_\nu C(\delta m_{np} - E_\nu) Z(\delta m_{np} - E_\nu, E_\nu) \\
\times E_\nu^2(\delta m_{np} - E_\nu) \sqrt{(\delta m_{np} - E_\nu)^2 - m_e^2} \\
\times [f_{\bar{\nu}_e}(E_\nu)] [f_{e^-}(\delta m_{np} - E_\nu)]. \quad (24)
\end{aligned}$$

$C(E_e)$  and  $Z(E_e, E_\nu)$  are modifications to the integrand from Coulomb corrections and zero-temperature radiative corrections, respectively, for charged-lepton-energy argument  $E_e$ . The quantities  $f_i$  give the lepton occupation numbers for  $i = \nu_e, \bar{\nu}_e, e^-, e^+$ . In this work, the occupation numbers are always assumed to be FD in character

$$f_i^{(\text{FD})}(E; T_i, \mu_i) = \frac{1}{e^{(E-\mu_i)/T_i} + 1}. \quad (25)$$

We use  $T_{\text{cm}}$  for the temperature quantity in the neutrino occupation numbers, and  $T$  for the plasma temperature in the charged lepton occupation numbers. In addition, we evolve the electron chemical potential,  $\mu_e$ , for use in the electron occupation numbers. The positron chemical potential is always assumed to be equal in magnitude and opposite in sign of the electron chemical potential. We take the electron neutrino and antineutrino chemical potentials to be zero. Our expressions for the  $n \leftrightarrow p$  rates in Eqs. (19) – (24) are identical to those of Ref. [38] except they contain the zero-temperature radiative corrections of Ref. [32], a different notation for the weak coefficient in front of the integral, and some corrections to typographical errors.

We used the same set of approximations to simplify  $\langle |\mathcal{M}|^2 \rangle$  present in Eqs. (19) – (24). The result of this set of approximations is that the same coefficient is in front of the integral over  $E_\nu$ , namely  $G_F^2(1+3g_A^2)/2\pi^3$ , for all six rates in Eqs. (19) – (24). We do not explicitly calculate this coefficient in our code using currently accepted values of  $G_F$  and  $g_A$ . As an alternative, we can solve



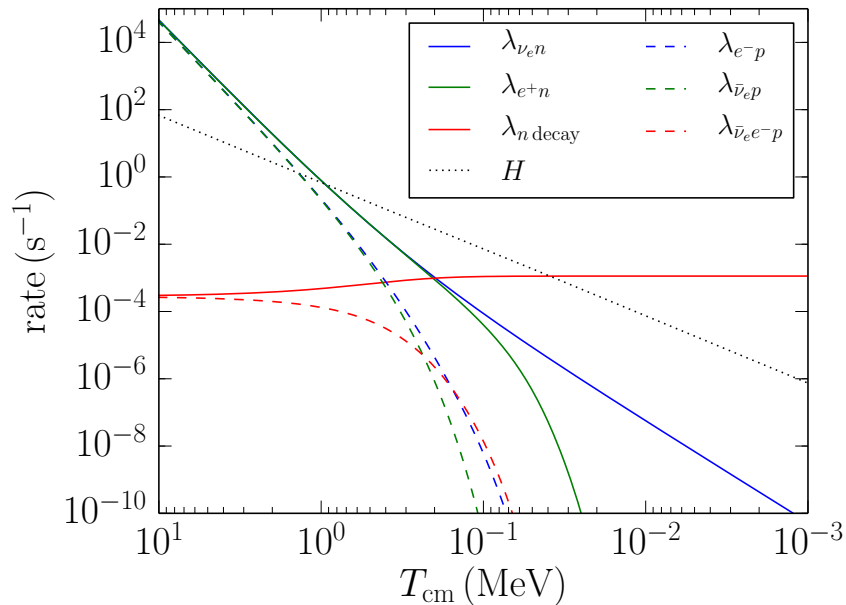


Figure 1: Rates as a function of comoving temperature parameter  $T_{\text{cm}}$ . The  $n \leftrightarrow p$  rates,  $\lambda$ , include all six processes in (1) – (6). Also plotted is the Hubble rate,  $H$ , for comparison. Our adopted neutron lifetime is  $\tau_n = 885.1$  s.

for the coefficient using the free neutron mean lifetime in vacuum,  $\tau_n$ , which we simply refer to as the neutron lifetime. The expression for the vacuum decay rate of free neutrons is

$$\frac{1}{\tau_n} = \frac{G_F^2(1 + 3g_A^2)}{2\pi^3} \int_0^{\delta m_{np} - m_e} dE_\nu C(\delta m_{np} - E_\nu) Z(\delta m_{np} - E_\nu, E_\nu) \times E_\nu^2 (\delta m_{np} - E_\nu) \sqrt{(\delta m_{np} - E_\nu)^2 - m_e^2}, \quad (26)$$

Eq. (26) is identical to Eq. (21) with  $f_{\bar{\nu}_e, e^-}(E) = 0$ . We can solve Eq. (26) for the coefficient  $G_F^2(1 + 3g_A^2)/(2\pi^3)$  in terms of  $\tau_n$  and a number for the phase-space integral. Ref. [39] gives the neutron lifetime as  $\tau_n = 882.5 \pm 2.1$  s, and Ref. [40] gives  $887.7 \pm 3.1$  s. As an average, we will take  $\langle \tau_n \rangle = 885.1$  s.

### 3. Results

Figure 1 shows a plot of each of the six rates in Eqs. (19) – (24) versus  $T_{\text{cm}}$ . For comparison purposes, the Hubble expansion rate ( $H$ ) is also plotted. The solid (dashed) curves gives the rates for the neutron destruction (creation)

processes. In all three reactions, the rate of neutron destruction is larger than that for creation. We can determine the difference in strength between neutron destruction and creation if we examine the explicit expressions in Eqs. (19) – (24). Consider first the rates for free neutron decay and the inverse three-body process, Eqs. (21) and (24) respectively. The equations are identical except for the expressions with the FD occupation numbers. Eq. (24) is proportional to the occupation numbers  $[f_{\bar{\nu}_e, e^-}]$  directly, as opposed to Eq. (21) which is proportional to the blocking factors  $[1 - f_{\bar{\nu}_e, e^-}]$ . For zero chemical potential, which is the case for the neutrinos,  $[1 - f(E)] \geq f(E)$  for all values of  $E$  if we assume FD occupation numbers as in Eq. (25). Therefore, the rate for free neutron decay is enhanced compared to the rate for the three-body process with regard to the neutrino occupation number contribution. The previous argument does not readily apply to the electron occupation numbers because the electron sea has a positive chemical potential. However, the chemical potential is on order the baryon number multiplied by the temperature at early times. The argument in the exponential of the occupation number is  $(E - \mu_e)/T \approx E/T - 10^{-9}$  implying that for energies  $E > 10^{-9}T$ , the blocking factor is larger than the stand-alone occupation number. Therefore, the electron and electron antineutrino occupation numbers give rise to the difference in strength between the two rates:  $\lambda_{n \text{ decay}} \geq \lambda_{\bar{\nu}_e e^- p}$  at all temperatures in Fig. 1.

The above argument for the difference in strength of the  $n \leftrightarrow p \bar{\nu}_e e^-$  rates is not immediately applicable to the two capture reactions,  $\nu_e n \leftrightarrow p e^-$  and  $e^+ n \leftrightarrow p \bar{\nu}_e$ . There is a reactant and product lepton in all four capture processes, so we cannot directly compare  $f_i f_j$  to  $[1 - f_i][1 - f_j]$  like we did in Eqs. (21) and (24). The key to understanding the comparative strength of the neutron destruction over creation rates is the threshold energy,  $E_{\text{thresh}}$ , absent in the destruction channel but present in the creation channel. The threshold energies are  $E_{\text{thresh}}^{(e)} = \delta m_{np}$  for the electron in process (4) and  $E_{\text{thresh}}^{(\nu)} = \delta m_{np} + m_e$  for the electron antineutrino in process (5). In either capture reaction,  $f(E \sim E_{\text{thresh}})$  is strictly less than  $[1 - f(E \sim E_{\text{thresh}})]$  for the lepton requiring a threshold energy. For the lepton which does not require a threshold energy ( $\nu_e$  in (1) and  $e^+$  in (2)),  $f(E \sim 0) \lesssim [1 - f(E \sim 0)]$ . The threshold energy reduces the allowed phase-space for the process to occur. At high temperatures, the threshold is negligible and the reduction in phase space minimal. The neutron creation rate is equal to the destruction rate as seen in the high-temperature range of Fig. 1. At lower temperatures, the rates begin to diverge once the threshold becomes significant.

The neutron destruction rates are larger than the corresponding creation rates for either the capture reactions or free neutron decay. The result is a decrease in the neutron abundance. Standard BBN produces mostly  $^1\text{H}$  and  $^4\text{He}$ . The neutrons which survive WFO will become bound in the  $^4\text{He}$  isotope. Therefore, when investigating altered scenarios of WFO, the principal cosmological observable we will monitor is the primordial mass fraction of  $^4\text{He}$ , namely  $Y_P \equiv 4Y_{^4\text{He}}$  and not to be confused with the free proton abundance  $Y_p$ . We use our adopted value of the neutron lifetime,  $\tau_n = 885.1 \text{ s}$ , to obtain a  $Y_P$  baseline

of

$$Y_P^{(\text{base})}[\tau_n = 885.1 \text{ s}] = 0.2477. \quad (27)$$

### 3.1. First scenario

In Fig. 1,  $\lambda_{n \text{ decay}}$  is not constant with  $T_{\text{cm}}$ . In medium, free neutron decay is inhibited by the FD blocking factors  $[1 - f_{\bar{\nu}_e}]$  and  $[1 - f_{e^-}]$ . Blocking reduces  $\lambda_{n \text{ decay}}$ , as shown in Fig. 2. In vacuum we drop the FD blocking factors [like we did in Eq. (26)], but in medium we must include them. At high temperatures, the FD occupation numbers for both  $e^-$  and  $\bar{\nu}_e$  are  $\sim 0.5$  for the range of energy values  $0 < E < \delta m_{np}$ . Therefore, the FD blocking factors are each  $\sim 0.5$  and the overall rate for  $\lambda_{n \text{ decay}}$  is  $\sim 0.25$  the vacuum rate. This is evident in Fig. 2 where the value of  $\lambda_{n \text{ decay}}$  at high temperature is a factor of four lower than the value at low temperature. Eventually, the free neutron decay rate converges to the vacuum rate at  $T_{\text{cm}} \sim 100 \text{ keV}$ , implying that FD blocking is negligible at this epoch. However,  ${}^4\text{He}$  formation occurs during this  $T_{\text{cm}} \sim 100 \text{ keV}$  epoch. In-medium free neutron decay is the dominant weak isospin-changing process before  ${}^4\text{He}$  nuclei form, as shown in Fig. 1. Modifications to the free neutron decay rate at late epochs,  $300 \text{ keV} \gtrsim T_{\text{cm}} \gtrsim 100 \text{ keV}$ , will alter the  $n/p$  ratio and produce changes in  $Y_P$ . If  $\lambda_{n \text{ decay}} \leq 1/\tau_n$ , then we would expect more neutrons to survive into the BBN epoch. The net result should be an increase in  $Y_P$  compared to the scenario  $\lambda_{n \text{ decay}} = 1/\tau_n$ .

The first scenario of altered WFO we investigate is the sensitivity of  $Y_P$  to in-medium free neutron decay and the role of phase-space blocking factors. Our procedure is as follows for this scenario. At high temperature we calculate all six of the  $n \leftrightarrow p$  rates using the expressions in Eqs. (19) – (24). Once  $T_{\text{cm}}$  reaches a user-specified temperature, we no longer calculate the free neutron decay rate using (21). At and below the specified temperature, we set the free neutron decay rate equal to the vacuum decay rate, namely  $\lambda_{n \text{ decay}} \rightarrow 1/\tau_n$ , in essence ignoring the FD blocking factors  $[1 - f_{\bar{\nu}_e, e^-}]$  in Eq. (21). We include and calculate the three-body rate,  $\lambda_{\bar{\nu}_e e^- p}$ , at all temperatures. Excluding the three-body rate produces a relative change of  $\sim 1.5 \times 10^{-3}$  in  $Y_P$  and has little effect for  $T_{\text{cm}} \lesssim 300 \text{ keV}$ . Within our code, we implement the following rate expressions, denoted  $\lambda^{(\text{Sc. 1})}$  for this first scenario

$$\lambda_{n \text{ decay}}^{(\text{Sc. 1})}(T_{\text{cm}}) = \begin{cases} \lambda_{n \text{ decay}} & \text{if } T_{\text{cm}} > T_{\text{WFO}} \\ 1/\tau_n & \text{if } T_{\text{cm}} < T_{\text{WFO}} \end{cases}, \quad (28)$$

$$\lambda_i^{(\text{Sc. 1})}(T_{\text{cm}}) = \lambda_i,$$

where  $i = \nu_e n, e^+ n, e^- p, \bar{\nu}_e p, \bar{\nu}_e e^- p$  for the rates in Eqs. (19), (20), (22), (23), (24).  $T_{\text{WFO}}$  is the user-specified “weak freeze-out temperature.”

Figure 3 shows the relative difference in  $Y_P$  plotted against  $T_{\text{WFO}}$  for a neutron lifetime  $\tau_n = 885.1 \text{ s}$  in the first scenario. The relative difference,  $\delta Y_P$ , is with respect to the  $Y_P$  baseline in Eq. (27)

$$\delta Y_P = \frac{Y_P - Y_P^{(\text{base})}[\tau_n = 885.1 \text{ s}]}{Y_P^{(\text{base})}[\tau_n = 885.1 \text{ s}]}. \quad (29)$$

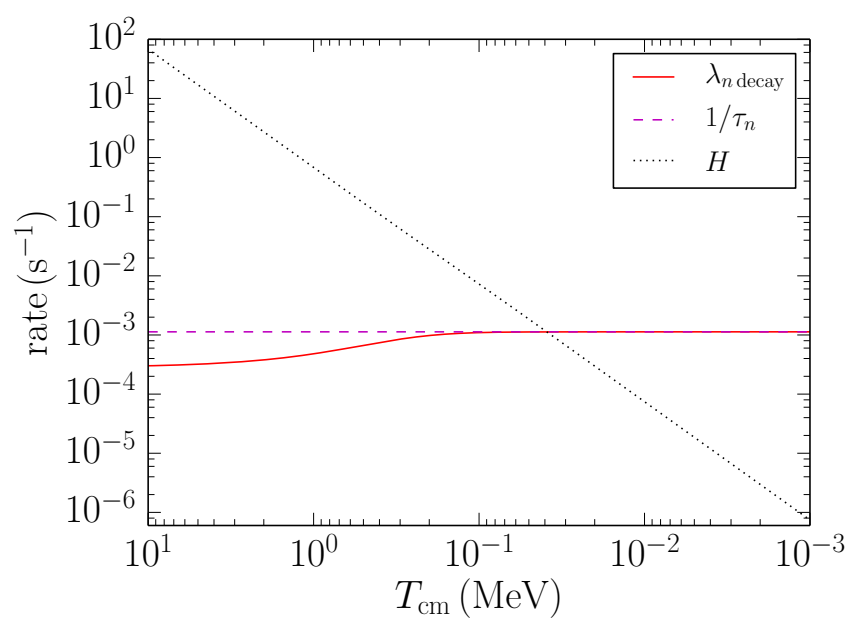


Figure 2: The in-medium free neutron decay rate,  $\lambda_{n \text{ decay}}$ , as a function of the comoving temperature parameter  $T_{\text{cm}}$ . Also plotted is the Hubble expansion rate,  $H$ , and the vacuum neutron decay rate,  $1/\tau_n$ , for comparison. Note that phase-space blocking decreases  $\lambda_{n \text{ decay}}$  relative to the vacuum neutron decay rate at temperatures  $T_{\text{cm}} \gtrsim 100 \text{ keV}$ . Our adopted neutron lifetime is  $\tau_n = 885.1 \text{ s}$ .

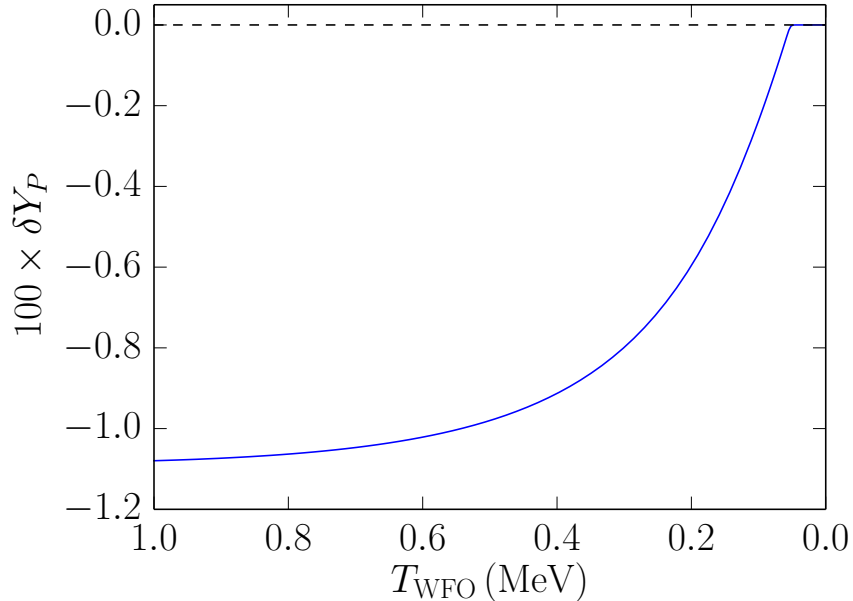


Figure 3: The relative difference in  $Y_P$  compared to the baseline [Eq. (29)] as a function of  $T_{\text{WFO}}$  in the first scenario of altered WFO. All six processes utilize the expressions in Eqs. (19) – (24) until  $T_{\text{cm}}$  reaches the user-specified  $T_{\text{WFO}}$ . For  $T_{\text{cm}} < T_{\text{WFO}}$ , the free neutron decay rate is set to the vacuum rate,  $1/\tau_n$ . Our adopted neutron lifetime is  $\tau_n = 885.1$  s.

The first scenario is able to induce a change in  $Y_P$  at the percent level. The rates for the capture processes are proportional to  $T_{\text{cm}}^5$  for high temperature, implying that the free neutron decay rate has a vanishingly small contribution in effecting the  $n/p$  ratio in this regime. As a result, the scenario of altered WFO considered here is immutable for  $T_{\text{WFO}} \gtrsim$  a few MeV and the curve in Fig. 3 begins to asymptote as  $T_{\text{WFO}}$  increases into this range of comoving temperature parameter.

The first altered scenario of WFO has no effect for values of  $T_{\text{WFO}}$  set after  ${}^4\text{He}$  formation,  $T_{\text{cm}} \lesssim 50$  keV, and the relative change in  $Y_P$  is zero as shown in Fig. 3. In addition,  $\delta Y_P$  has asymptoted for  $T_{\text{cm}} \gtrsim 1$  MeV.  $\delta Y_P$  undergoes a rapid ascent for the range  $400$  keV  $\gtrsim T_{\text{cm}} \gtrsim 100$  keV and connects the high and low temperature plateaus for the first scenario. This range encompasses the epoch when  $\lambda_{n \text{ decay}}$  is roughly the same order of magnitude as  $\lambda_{\nu_e n}$  and  $\lambda_{e+n}$  according to Fig. 1. Furthermore, the steep slope of  $\delta Y_P$  as a function of  $T_{\text{WFO}}$  gives us information on *when* the  $n/p$  ratio, and by extension  $Y_P$ , is the most mutable to the free neutron decay rate. In this first scenario of altered WFO, we have abruptly changed the free neutron decay rate to the vacuum value. Over the entire history of the early universe, the free neutron decay rate only

changes by a factor of 4, larger than the change imposed by the first scenario. Nevertheless, the small temperature range  $400 \text{ keV} \gtrsim T_{\text{cm}} \gtrsim 100 \text{ keV}$ , which is  $\sim 15$  Hubble times, has an impact on WFO at the percent level in the first scenario.

### 3.2. Second scenario

Figure 1 shows that at  $T_{\text{cm}} \sim 1 \text{ MeV}$ , the neutron destruction rates ( $\lambda_{\nu_e n}$ ,  $\lambda_{\bar{\nu}_e n}$ ) are roughly an order of magnitude larger than the neutron creation rates ( $\lambda_{e^- p}$ ,  $\lambda_{\bar{\nu}_e p}$ ). Both of the neutron creation rates require a threshold energy for the incident lepton, reducing the amount of accessible phase space and lowering the value of the rates compared to the neutron destruction rates. In the second scenario of altered WFO, we will neglect the processes which require a threshold for  $T_{\text{cm}} < T_{\text{WFO}}$ . This is equivalent to an instantaneous WFO epoch for the two lepton capture rates on protons, Eqs. (22) and (23).

Our procedure for this scenario is similar to that of the first. We calculate all six  $n \leftrightarrow p$  rates at high temperature. Once  $T_{\text{cm}}$  is lower than  $T_{\text{WFO}}$ , we neglect the lepton capture rates on protons in Eqs. (22) and (23). The expressions implemented in the code are

$$\lambda_i^{(\text{Sc. 2})}(T_{\text{cm}}) = \begin{cases} \lambda_i & \text{if } T_{\text{cm}} > T_{\text{WFO}} \\ 0 & \text{if } T_{\text{cm}} < T_{\text{WFO}} \end{cases},$$

$$\lambda_j^{(\text{Sc. 2})}(T_{\text{cm}}) = \lambda_j, \quad (30)$$

where  $\lambda_i$  are the expressions for the capture rates on protons in Eqs. (22) and (23). The other four  $n \leftrightarrow p$  rates use the expressions  $\lambda_j$  in Eqs. (19), (20), (21), and (24) at all temperatures.

Figure 4 shows the results of the second scenario. The neutron lifetime is fixed at  $\tau_n = 885.1 \text{ s}$ . The horizontal axis gives  $T_{\text{WFO}}$  and the vertical axis gives the relative change in  $Y_P$  from the baseline in Eq. (27). If we neglect the capture rates on protons at  $T_{\text{WFO}} \sim 1 \text{ MeV}$ , we find a  $\sim 40\%$  decrease in  $Y_P$ . The relative difference in  $Y_P$  decreases with decreasing  $T_{\text{WFO}}$ . At  $T_{\text{WFO}} \sim 400 \text{ keV}$ , there exists a  $\sim 1\%$  change in  $Y_P$ . This corresponds to an epoch where the capture rates on protons are roughly two orders of magnitude smaller than the capture rates on neutrons. The average energy of neutrinos at this epoch is  $\sim 1.2 \text{ MeV}$ , only two-thirds of the value of  $\delta m_{np} + m_e$ . Only neutrinos in the tail of the distribution have enough energy to contribute to process (5). The exclusion of process (5), and to a greater extent process (4), leads to a noticeable change well below our initial estimate for WFO,  $T_{\text{cm}} \sim T_{\text{eq}}$ .

### 3.3. Third scenario

In Fig. 1,  $\lambda_{\nu_e n} \sim H$  for  $T_{\text{cm}} \sim 1.0 \text{ MeV}$ , in line with our earlier estimate for  $T_{\text{eq}}$ . For  $T_{\text{cm}} < T_{\text{eq}}$ , the Hubble expansion rate is larger than any of the  $n \leftrightarrow p$  rates until  $T_{\text{cm}} \simeq 50 \text{ keV}$ , where  $\lambda_{n \text{ decay}}$  becomes larger than  $H$ . In the third scenario of altered WFO, we will implement an even more extreme instantaneous WFO as compared to the second scenario.

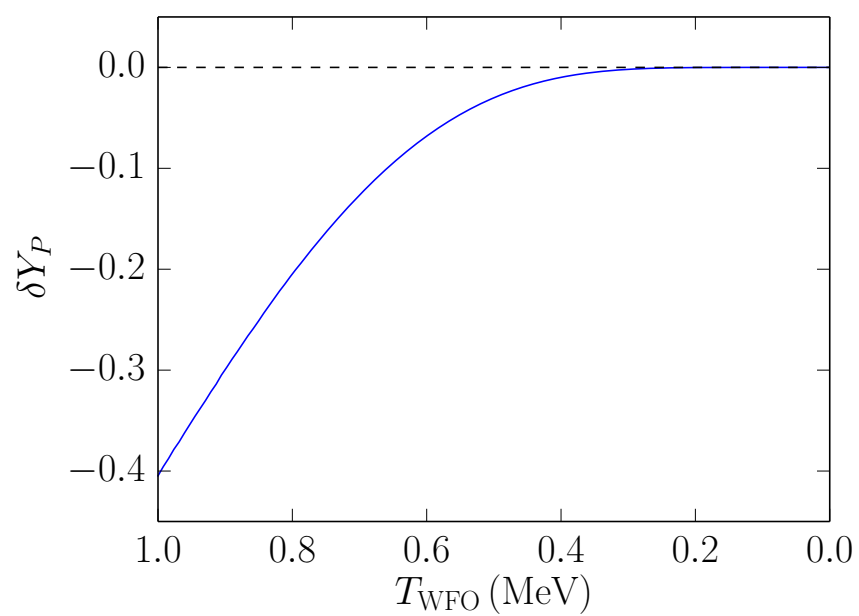


Figure 4: The relative difference in  $Y_P$  compared to the baseline [Eq. (29)] as a function of  $T_{\text{WFO}}$  in the second scenario of altered WFO. All six processes utilize the expressions in Eqs. (19) – (24) until  $T_{\text{cm}}$  reaches the user-specified  $T_{\text{WFO}}$ . For  $T_{\text{cm}} < T_{\text{WFO}}$ , the capture rates on protons, namely  $e^- p \rightarrow n + \nu_e$  and  $\bar{\nu}_e p \rightarrow n e^+$ , are set to zero. The neutron lifetime is  $\tau_n = 885.1$  s.

At high temperature we calculate all six of the  $n \leftrightarrow p$  rates using the expressions in Eqs. (19) – (24). Once  $T_{\text{cm}}$  reaches  $T_{\text{WFO}}$  we no longer calculate the rates associated with the lepton capture processes on protons *and* neutrons, i.e. processes (1), (2), (4), and (5), thereby instituting an instantaneous freeze-out of those specific four lepton capture reactions. We will calculate and include the in-medium free neutron decay rate and associated inverse rate for all temperatures in this scenario. The expression implemented in the code is

$$\lambda_i^{(\text{Sc. 3})}(T_{\text{cm}}) = \begin{cases} \lambda_i & \text{if } T_{\text{cm}} > T_{\text{WFO}} \\ 0 & \text{if } T_{\text{cm}} < T_{\text{WFO}} \end{cases},$$

$$\lambda_j^{(\text{Sc. 3})}(T_{\text{cm}}) = \lambda_j, \quad (31)$$

where  $\lambda_i$  are the expressions for the capture rates in Eqs. (19), (20), (22), and (23); and  $\lambda_j$  are the expressions in Eqs. (21) and (24).

Figure 5 gives the results of the WFO approximation in the third scenario. In this scenario, we define the relative change in  $Y_P$  as the following

$$\delta Y_P = \frac{Y_P - Y_P^{(\text{base})}[\tau_n]}{Y_P^{(\text{base})}[\tau_n]}, \quad (32)$$

where  $Y_P^{(\text{base})}[\tau_n]$  is the baseline value of  $Y_P$  at a given  $\tau_n$  if we set  $T_{\text{WFO}} = 0$ . The top panel of Fig. 5 shows contours of constant  $\delta Y_P$  in the  $T_{\text{WFO}}$  vs.  $\tau_n$  plane. The bottom panel shows the baseline values,  $Y_P^{(\text{base})}$ . The contours in the top panel are roughly horizontal, indicating that the relative changes in  $Y_P$  are independent of  $\tau_n$ . Our estimate for  $T_{\text{eq}}$  was 0.9 MeV. If we set  $T_{\text{WFO}} = T_{\text{eq}}$ , we see that our calculation for  $Y_P$  induces a  $\sim 50\%$  increase over the baseline. When calculating  $\delta Y_P$  for the second scenario, we found a comparable 35% *decrease* in  $Y_P$  from the baseline when  $T_{\text{WFO}} = T_{\text{eq}}$  in Fig. 4. The exclusion of the capture rates on neutrons in going from scenario 2 to scenario 3 results in a nearly 100% shift in  $Y_P$ . In Fig. 1, the capture rates are four orders of magnitude larger than the free-neutron decay rate when  $T_{\text{cm}} = T_{\text{eq}}$ . Neglecting the capture rates leads to a significantly different history of WFO. The instantaneous WFO approximation improves if we lower  $T_{\text{WFO}}$ . However, even at  $T_{\text{WFO}} = 100$  keV, a  $\sim 1\%$  relative difference in  $Y_P$  persists.

Figure 6 shows the evolution of the  $n/p$  ratio as a function of  $T_{\text{cm}}$  for different values of  $T_{\text{WFO}}$  within the third scenario. A curve assuming the  $n/p$  ratio stays in weak equilibrium is included for comparison. For each nonzero  $T_{\text{WFO}}$ , the  $n/p$  ratio starkly diverges from the baseline curve at that value of  $T_{\text{WFO}}$ . The value of the  $n/p$  ratio is a monotonic function of  $T_{\text{WFO}}$ , approaching the baseline for decreasing values of  $T_{\text{WFO}}$ . The evolution of the  $n/p$  ratio abruptly ceases at  $T_{\text{cm}} \sim 50$  keV - the conclusion of  ${}^4\text{He}$  formation.

The value of the  $n/p$  ratio is important for BBN. Before BBN commences, the abundances are in nuclear statistical equilibrium. For a nucleus with mass number  $A$  and atomic number  $Z$ , the NSE abundance is [8]

$$Y_X^{(\text{NSE})} \simeq Y_p^Z Y_n^{A-Z} 2^{(A-3)/2} \pi^{3(A-1)/2} g_X A^{3/2} \left[ \frac{n_b}{(T m_b)^{3/2}} \right]^{A-1} e^{B_X/T}, \quad (33)$$



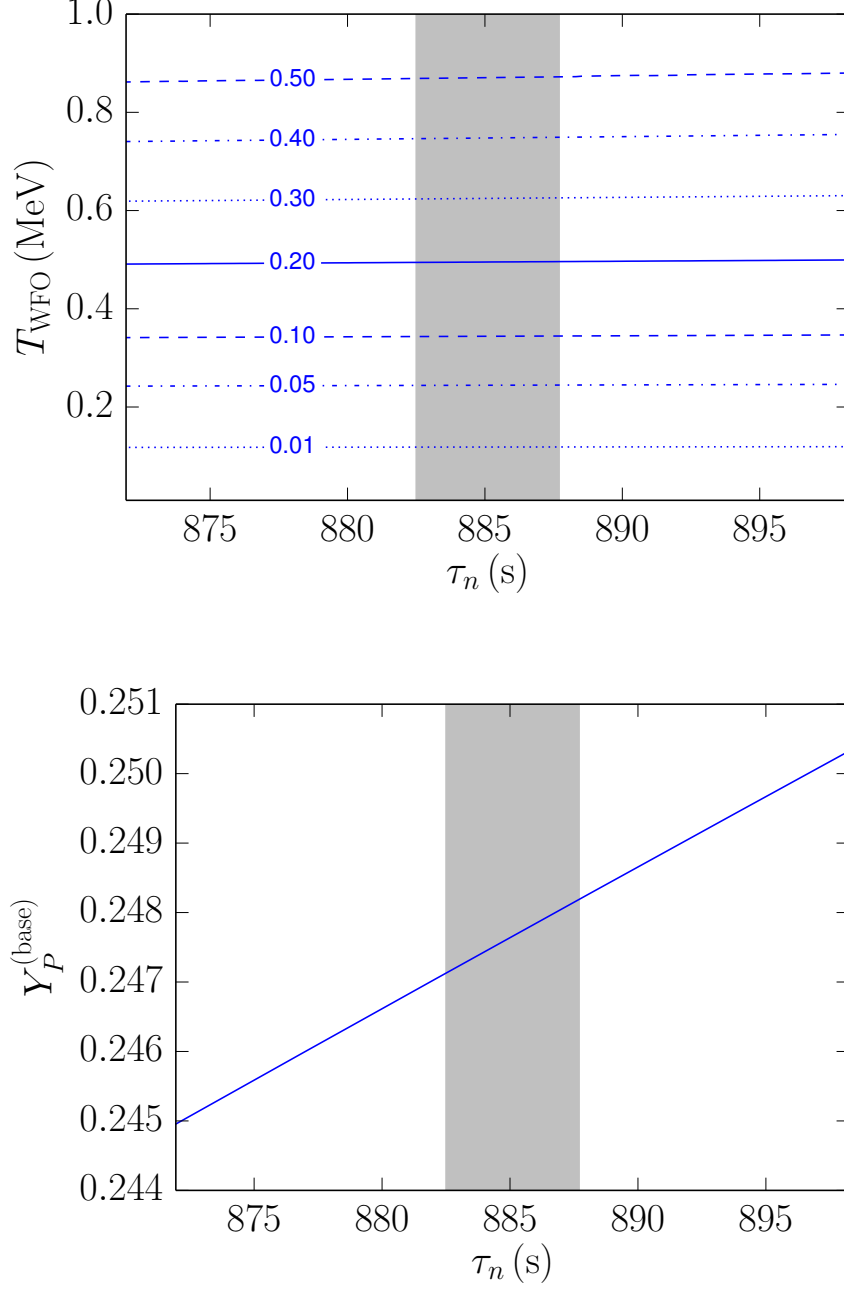


Figure 5: (Top)  $T_{\text{WFO}}$  plotted against  $\tau_n$  for contours of constant  $\delta Y_P$  in the third scenario of altered WFO. Here, the relative difference in  $Y_P$  is given in Eq. (32), where the baseline value of  $Y_P$  changes with  $\tau_n$ . All six processes utilize the expressions in Eqs. (19) – (24) until  $T_{\text{cm}}$  reaches the user-specified  $T_{\text{WFO}}$ . For  $T_{\text{cm}} < T_{\text{WFO}}$ , the four capture rates, namely  $\nu_e + n \leftrightarrow e^- p$  and  $e^+ n \leftrightarrow \bar{\nu}_e p$ , are set to zero. (Bottom) The baseline values of  $Y_P$  for a given  $\tau_n$ . For the baseline, we set  $T_{\text{WFO}} = 0$ . In both panels the shaded silver vertical region is the one-sigma estimate for  $\tau_n = 885.1 \pm 2.6$  s calculated from Refs. [39, 40]

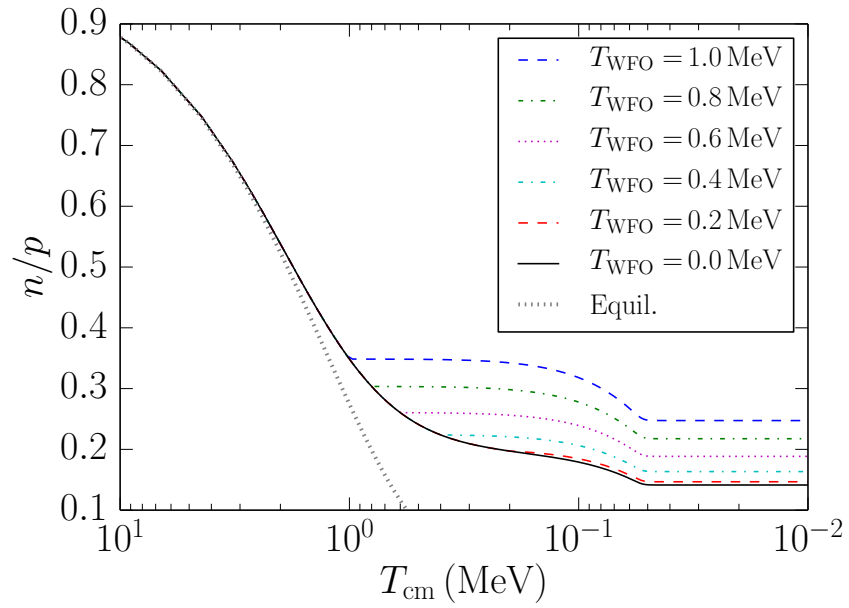


Figure 6: The  $n/p$  ratio as a function of comoving temperature parameter  $T_{\text{cm}}$  in the third scenario of altered WFO, the same as in Fig. 5. Each  $T_{\text{WFO}}$  curve represents a different value for temperature  $T_{\text{cm}} = T_{\text{WFO}}$  where processes (1), (2), (4), and (5) are sharply turned off. All curves use  $\tau_n = 885.1$  s. Also included is a curve (Equil.) assuming the  $n/p$  ratio stays in weak equilibrium, i.e.  $n/p = e^{-\delta m_{np}/T}$ , where we neglect the electron chemical potential and set the neutrino chemical potential to zero.

In Eq. (33),  $g_X$  is the spin and  $B_X$  is the binding energy of nucleus  $X$ .  $m_b$  is the baryon rest mass energy. We can relate the baryon number density to the entropy per baryon in the plasma

$$s_{\text{pl}} = \frac{1}{n_b} \frac{2\pi^2}{45} g_{*S} T^3, \quad (34)$$

where  $g_{*S}$  is the statistical entropic weight [31].  $s_{\text{pl}}$  is nearly constant during WFO (see Ref. [11] for a discussion of entropy flows during the weak decoupling, WFO, and BBN epochs). Eq. (33) shows that  $Y_X$  depends on time/temperature through the quantities  $Y_p^Z$ ,  $Y_n^{A-Z}$ , and  $T^{9(1-A)/2}$  before the abundance goes out of equilibrium. As a result,  $Y_X$  will depart from NSE at specific values of  $Y_p$  and  $Y_n$ , or equivalently, at a specific value of the  $n/p$  ratio. The evolution of  $Y_X$  then proceeds to follow from a Boltzmann equation. The Boltzmann equation is sensitive to the initial conditions, which include the  $n/p$  ratio in this case.

Figure 7 shows the evolution of the primordial abundances as functions of  $T_{\text{cm}}$ . The dashed curves correspond to the baseline case,  $T_{\text{WFO}} = 0$ , whereas the solid curves correspond to the case  $T_{\text{WFO}} = 1.0 \text{ MeV}$  in the third scenario. Although the vertical axis ranges over 36 orders of magnitude, the instantaneous WFO approximation induces a discernible difference on the evolution of the abundances. Furthermore, the solid and dashed curves begin diverging for  $T_{\text{cm}} \lesssim 1.0 \text{ MeV}$ , the  $T_{\text{WFO}}$  value for the solid curves.  ${}^4\text{He}$  is still in NSE at  $T_{\text{cm}} = 1.0 \text{ MeV}$ . In essence, we have precipitated an earlier epoch of out-of-equilibrium evolution when we set  $T_{\text{WFO}} = 1.0 \text{ MeV}$ . Therefore, we have a different  $n/p$  ratio and initial condition as dictated by Eq. (33) compared to the baseline case. The result is a different evolution for  ${}^4\text{He}$ . The helium abundances differ by  $\sim 50\%$  for the two cases at the conclusion of BBN.  ${}^4\text{He}$  is indeed sensitive to the  $n/p$  ratio, but to a lesser extent so are deuterium and  ${}^3\text{He}$ . For this scenario compared to the baseline, deuterium differs by  $\sim 44\%$  and  ${}^3\text{He}$  differs by  $\sim 14\%$ .

#### 3.4. Fourth scenario

For the fourth and last scenario, we combine scenarios 1 and 3. The expression for the rates in the code is

$$\begin{aligned} \lambda_i^{(\text{Sc. 4})}(T_{\text{cm}}) &= \begin{cases} \lambda_i & \text{if } T_{\text{cm}} > T_{\text{WFO}} \\ 0 & \text{if } T_{\text{cm}} < T_{\text{WFO}} \end{cases}, \\ \lambda_{n \text{ decay}}^{(\text{Sc. 4})}(T_{\text{cm}}) &= \begin{cases} \lambda_{n \text{ decay}} & \text{if } T_{\text{cm}} > T_{\text{WFO}} \\ 1/\tau_n & \text{if } T_{\text{cm}} < T_{\text{WFO}} \end{cases}, \\ \lambda_{\bar{\nu}_e e^- p}^{(\text{Sc. 4})}(T_{\text{cm}}) &= \lambda_{\bar{\nu}_e e^- p}, \end{aligned} \quad (35)$$

where  $\lambda_i$  are the expressions for the capture rates in Eqs. (19), (20), (22), and (23). In other words, in the fourth scenario we assume a sharp transition at a chosen  $T_{\text{WFO}}$  after which we neglect all lepton capture processes and use an unblocked, vacuum decay rate for free neutrons.

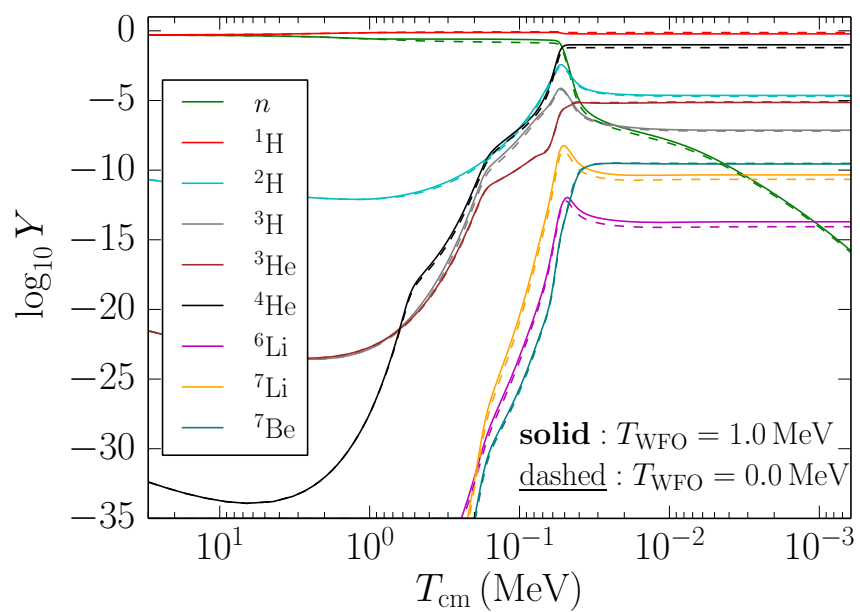


Figure 7: The abundances as a function of comoving temperature parameter  $T_{\text{cm}}$  in the third scenario of altered WFO, the same as in Fig. 5. The solid lines show the abundances if  $T_{\text{WFO}} = 1.0 \text{ MeV}$ . The dashed lines show the abundances if  $T_{\text{WFO}} = 0.0 \text{ MeV}$ , i.e. if the  $n \leftrightarrow p$  rates are calculated at all times. The neutron lifetime is  $\tau_n = 885.1 \text{ s}$ .

Figure 8 shows the relative change in  $Y_P$  plotted against  $T_{\text{WFO}}$ . Scenario 1 produced a decrease in  $Y_P$ , and scenario 3 produced an increase in  $Y_P$  over the baseline. In addition, scenario 3 produced much larger changes in  $Y_P$  for equal  $T_{\text{WFO}}$ . As a result,  $\delta Y_P$  for this scenario seen in Fig. 8 closely follows that of the third scenario. If we consider the top panel of Fig. 5, we see a  $\sim 60\%$  change in  $Y_P$  for  $T_{\text{WFO}} = 1.0 \text{ MeV}$  at the central value  $\tau_n = 885.1 \text{ s}$ . This is in line with the change at  $T_{\text{WFO}} = 1.0 \text{ MeV}$  for scenario 4 in Fig. 8. To be more precise,  $\delta Y_P$  for scenario 4 is a half percent lower than scenario 3 for  $T_{\text{WFO}} = 1.0 \text{ MeV}$ . At  $T_{\text{WFO}} = 1.0 \text{ MeV}$  in scenario 1,  $Y_P$  is more than a full percent lower than the baseline. The values for  $\delta Y_P$  in scenario 4 are not perfect incoherent sums of the values in scenarios 1 and 3, but are also not widely discrepant. At lower temperatures, the effect from the blocking factors in free neutron decay play a lesser role than they do at higher temperatures. As a result, scenario 4 becomes equivalent to scenario 3 and  $\delta Y_P$  assume the same values for both scenarios at lower temperature. When  $T_{\text{WFO}} \sim 100 \text{ keV}$ , we find a  $\sim 1\%$  change in  $Y_P$  for both scenarios 3 and 4. Note that if we choose  $T_{\text{WFO}} = 0.7 \text{ MeV}$ , this scenario yields a  $Y_P$  nearly 40% above the baseline standard BBN value. Clearly, Fig. 8 shows that any choice of a sharp  $T_{\text{WFO}}$  in scenario 4 results in incorrect nucleosynthesis.

#### 4. Conclusion

We have presented calculations which show that neglecting almost any of the isospin-changing weak interaction processes in the WFO epoch is unjustified and results in incorrect BBN. In particular, the idea that there is a WFO temperature,  $T_{\text{WFO}}$ , below which lepton capture on neutrons and protons, and blocking factors for in-medium free neutron decay can be neglected, is inaccurate and misleading. We have quantified how the effect of individual isospin-changing weak interactions figures into the evolution of the  $n/p$  ratio and light-element abundances.

Most extant BBN calculations [15, 16, 17, 18] capture the physics of WFO correctly. It is nevertheless surprising that lepton capture reactions, even those with an energy threshold, are important in calculating final helium and deuterium abundances. Fig. 1 illustrates why this result is surprising. Note that in Fig. 1, the Hubble expansion rate dominates over all lepton capture isospin-changing reactions for  $T_{\text{cm}} < 0.9 \text{ MeV}$ , but the comparison between individual reaction rates and the Hubble expansion rate can be misleading. A more revealing procedure is to solve for the solution of the  $n/p$  ratio, tantamount to a solution of the two coupled first-order differential equations, (17) and (18). These solutions involve exponentials of integrals of the Hubble expansion rate convolved with isospin-changing weak interaction rates, as shown in Ref. [41] for the early universe and Ref. [42] for the very similar situation in a neutrino-driven wind around a hot proto-neutron star. In essence, these solutions show that the isospin-changing weak interactions have an integrated, cumulative effect which must be accounted for. Although these weak interaction rates drop

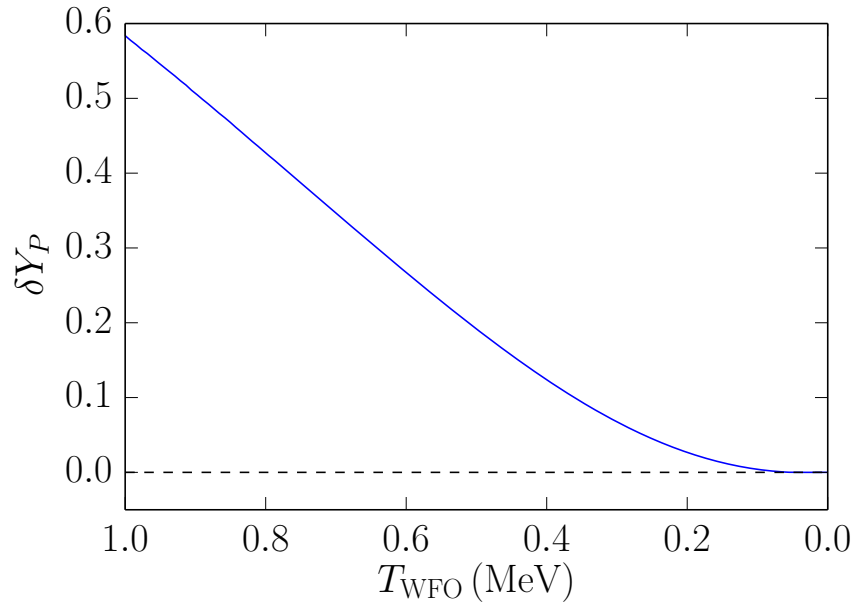


Figure 8: The relative difference in  $Y_P$  compared to the baseline [Eq. (29)] as a function of  $T_{\text{WFO}}$  in the fourth scenario of altered WFO. All six processes utilize the expressions in Eqs. (19) – (24) until  $T_{\text{cm}}$  reaches the user-specified  $T_{\text{WFO}}$ . For  $T_{\text{cm}} < T_{\text{WFO}}$ , the capture rates, namely  $e^-p \leftrightarrow n + \nu_e$  and  $\bar{\nu}_e p \leftrightarrow ne^+$ , are set to zero, and the free neutron decay rate is set to the vacuum rate. Our adopted neutron lifetime is  $\tau_n = 885.1$  s.

dramatically as the temperature drops, the Hubble expansion rate also drops - necessitating a numerical approach in integrating these rates.

Future prospects for high-precision determinations of the primordial abundances of helium, e.g., from cosmic microwave background stage 4 experiments [3], and deuterium, from thirty-meter-class telescopes [1, 2], heighten the prospects for BBN constraints on and probes of BSM physics in the early universe. Our results point up the sensitivity of BBN to slow, subdominant weak interaction processes at quite low temperatures,  $T \sim 100$  keV. In turn, this suggests that high precision measurements of light-element abundances can translate into constraints on the thermal physics and any neutrino sector or BSM physics that affects neutrino or charged-lepton distribution functions and number densities at this epoch. For example, neutrino oscillations [10, 43], sterile neutrinos [44], particle decay [45, 46, 47, 47, 48, 49, 50], and large neutrino magnetic moments [51], all can produce changes in active neutrino distributions, number densities, and overall energy density which can slightly or substantially affect the weak isospin-changing interactions we consider in this paper. The weak interaction physics we have considered in this paper suggests that BBN will be an even more sensitive probe of these and other BSM physics issues in the future.

## Acknowledgments

We thank Lauren Gilbert for useful conversations. We acknowledge the Integrated Computing Network at Los Alamos National Laboratory for super-computer time. This work was supported in part by NSF grant PHY-1307372 at UC San Diego.

## References

- [1] R. J. Cooke, M. Pettini, R. A. Jorgenson, M. T. Murphy, C. C. Steidel, Precision measures of the primordial abundance of deuterium, *The Astrophysical Journal* 781 (1) (2014) 31.
- [2] R. Cooke, M. Pettini, The primordial abundance of deuterium: ionization correction, *MNRAS* 455 (2016) 1512–1521. [arXiv:1510.03867](https://arxiv.org/abs/1510.03867), [doi:10.1093/mnras/stv2343](https://doi.org/10.1093/mnras/stv2343).
- [3] D. Green, Cosmology with CMB S4 workshop, [https://cosmo.uchicago.edu/CMB-S4workshops/index.php/UMICH-2015:Neutrino\\_and\\_Light\\_Relativistic\\_Species\\_Summary](https://cosmo.uchicago.edu/CMB-S4workshops/index.php/UMICH-2015:Neutrino_and_Light_Relativistic_Species_Summary), Accessed: 2015-11-11.
- [4] D. N. Schramm, M. S. Turner, Big-bang nucleosynthesis enters the precision era, *Reviews of Modern Physics* 70 (1998) 303–318. [arXiv:astro-ph/9706069](https://arxiv.org/abs/astro-ph/9706069), [doi:10.1103/RevModPhys.70.303](https://doi.org/10.1103/RevModPhys.70.303).
- [5] A. D. Dolgov, Neutrinos in cosmology, *Phys. Rep.* 370 (2002) 333–535. [arXiv:hep-ph/0202122](https://arxiv.org/abs/hep-ph/0202122), [doi:10.1016/S0370-1573\(02\)00139-4](https://doi.org/10.1016/S0370-1573(02)00139-4).

- [6] G. Steigman, Neutrinos And Big Bang Nucleosynthesis, ArXiv e-prints [arXiv:1208.0032](#).
- [7] R. H. Cyburt, B. D. Fields, K. A. Olive, T.-H. Yeh, Big bang nucleosynthesis: Present status, *Reviews of Modern Physics* 88 (1) (2016) 015004. [arXiv:1505.01076](#), [doi:10.1103/RevModPhys.88.015004](#).
- [8] E. M. Burbidge, G. R. Burbidge, W. A. Fowler, F. Hoyle, Synthesis of the Elements in Stars, *Reviews of Modern Physics* 29 (1957) 547–650. [doi:10.1103/RevModPhys.29.547](#).
- [9] A. D. Dolgov, S. H. Hansen, D. V. Semikoz, Non-equilibrium corrections to the spectra of massless neutrinos in the early universe, *Nuclear Physics B* 503 (1997) 426–444. [arXiv:hep-ph/9703315](#), [doi:10.1016/S0550-3213\(97\)00479-3](#).
- [10] G. Mangano, G. Miele, S. Pastor, T. Pinto, O. Pisanti, P. D. Serpico, Relic neutrino decoupling including flavour oscillations, *Nuclear Physics B* 729 (2005) 221–234. [arXiv:hep-ph/0506164](#), [doi:10.1016/j.nuclphysb.2005.09.041](#).
- [11] E. Grohs, G. M. Fuller, C. T. Kishimoto, M. W. Paris, A. Vlasenko, Neutrino energy transport in weak decoupling and big bang nucleosynthesis, *Phys. Rev. D* 93 (8) (2016) 083522. [arXiv:1512.02205](#), [doi:10.1103/PhysRevD.93.083522](#).
- [12] R. V. Wagoner, W. A. Fowler, F. Hoyle, On the Synthesis of elements at very high temperatures, *Astrophys.J.* 148 (1967) 3–49. [doi:10.1086/149126](#).
- [13] R. V. Wagoner, Synthesis of the Elements Within Objects Exploding from Very High Temperatures, *ApJS* 18 (1969) 247. [doi:10.1086/190191](#).
- [14] G. M. Fuller, C. J. Smith, Nuclear weak interaction rates in primordial nucleosynthesis, *Phys. Rev. D* 82 (12) (2010) 125017. [arXiv:1009.0277](#), [doi:10.1103/PhysRevD.82.125017](#).
- [15] E. Grohs, G. M. Fuller, C. T. Kishimoto, M. W. Paris, Probing neutrino physics with a self-consistent treatment of the weak decoupling, nucleosynthesis, and photon decoupling epochs, *J. Cosmology Astropart. Phys.* 5 (2015) 17. [arXiv:1502.02718](#).
- [16] L. Kawano, Let's go: Early universe 2. Primordial nucleosynthesis the computer way, NASA STI/Recon Technical Report 92 (1992) 25163.
- [17] O. Pisanti, A. Cirillo, S. Esposito, F. Iocco, G. Mangano, G. Miele, P. D. Serpico, PArthENoPE: Public algorithm evaluating the nucleosynthesis of primordial elements, *Computer Physics Communications* 178 (2008) 956–971. [arXiv:0705.0290](#), [doi:10.1016/j.cpc.2008.02.015](#).



- [18] A. Arbey, AlterBBN: A program for calculating the BBN abundances of the elements in alternative cosmologies, *Computer Physics Communications* 183 (2012) 1822–1831. [arXiv:1106.1363](#), [doi:10.1016/j.cpc.2012.03.018](#).
- [19] D. N. Blaschke, V. Cirigliano, Neutrino Quantum Kinetic Equations: The Collision Term, *ArXiv e-prints*[arXiv:1605.09383](#).
- [20] R. Barbieri, A. Dolgov, Neutrino oscillations in the early universe, *Nuclear Physics B* 349 (1991) 743–753. [doi:10.1016/0550-3213\(91\)90396-F](#).
- [21] E. K. Akhmedov, Z. G. Berezhiani, Implications of Majorana neutrino transition magnetic moments for neutrino signals from supernovae, *Nuclear Physics B* 373 (1992) 479–497. [doi:10.1016/0550-3213\(92\)90441-D](#).
- [22] G. Raffelt, G. Sigl, Neutrino flavor conversion in a supernova core, *Astroparticle Physics* 1 (1993) 165–183. [arXiv:astro-ph/9209005](#), [doi:10.1016/0927-6505\(93\)90020-E](#).
- [23] P. Strack, A. Burrows, Generalized Boltzmann formalism for oscillating neutrinos, *Phys. Rev. D* 71 (9) (2005) 093004. [arXiv:hep-ph/0504035](#), [doi:10.1103/PhysRevD.71.093004](#).
- [24] A. B. Balantekin, Y. Pehlivan, Neutrino neutrino interactions and flavour mixing in dense matter, *Journal of Physics G Nuclear Physics* 34 (2007) 47–65. [arXiv:astro-ph/0607527](#), [doi:10.1088/0954-3899/34/1/004](#).
- [25] C. Volpe, D. Väänänen, C. Espinoza, Extended evolution equations for neutrino propagation in astrophysical and cosmological environments, *Phys. Rev. D* 87 (11) (2013) 113010. [arXiv:1302.2374](#), [doi:10.1103/PhysRevD.87.113010](#).
- [26] A. B. Balantekin, G. M. Fuller, Neutrinos in cosmology and astrophysics, *Progress in Particle and Nuclear Physics* 71 (2013) 162–166. [arXiv:1303.3874](#), [doi:10.1016/j.pnpnp.2013.03.008](#).
- [27] A. de Gouvêa, S. Shalgar, Transition magnetic moments and collective neutrino oscillations: three-flavor effects and detectability, *J. Cosmology Astropart. Phys.* 4 (2013) 18. [arXiv:1301.5637](#), [doi:10.1088/1475-7516/2013/04/018](#).
- [28] J. Serreau, C. Volpe, Neutrino-antineutrino correlations in dense anisotropic media, *Phys. Rev. D* 90 (12) (2014) 125040. [arXiv:1409.3591](#), [doi:10.1103/PhysRevD.90.125040](#).
- [29] V. Cirigliano, G. M. Fuller, A. Vlasenko, A new spin on neutrino quantum kinetics, *Physics Letters B* 747 (2015) 27–35. [arXiv:1406.5558](#), [doi:10.1016/j.physletb.2015.04.066](#).

- [30] S. Dodelson, *Modern Cosmology*, Academic Press, Academic Press, 2003. URL <http://books.google.com/books?id=3oPRxdXJexcC>
- [31] E. W. Kolb, M. S. Turner, *The Early Universe.*, Addison-Wesley Publishing Co., 1990.
- [32] D. A. Dicus, E. W. Kolb, A. M. Gleeson, E. C. G. Sudarshan, V. L. Teplitz, M. S. Turner, Primordial nucleosynthesis including radiative, Coulomb, and finite-temperature corrections to weak rates, *Phys. Rev. D* 26 (1982) 2694–2706. doi:10.1103/PhysRevD.26.2694.
- [33] J.-L. Cambier, J. R. Primack, M. Sher, Finite temperature radiative corrections to neutron decay and related processes, *Nucl. Phys. B* 209 (1982) 372–388. doi:10.1016/0550-3213(82)90262-0.
- [34] R. E. Lopez, M. S. Turner, Precision prediction for the big-bang abundance of primordial  $^4\text{He}$ , *Phys. Rev. D* 59 (10) (1999) 103502. arXiv:astro-ph/9807279, doi:10.1103/PhysRevD.59.103502.
- [35] G. M. Fuller, W. A. Fowler, M. J. Newman, Stellar weak-interaction rates for sd-shell nuclei. I - Nuclear matrix element systematics with application to Al-26 and selected nuclei of importance to the supernova problem, *ApJS* 42 (1980) 447–473. doi:10.1086/190657.
- [36] C. J. Smith, G. M. Fuller, Weak interaction rate Coulomb corrections in big bang nucleosynthesis, *Phys. Rev. D* 81 (6) (2010) 065027. arXiv:0905.2781, doi:10.1103/PhysRevD.81.065027.
- [37] R. E. Lopez, M. S. Turner, G. Gyuk, Effect of finite nucleon mass on primordial nucleosynthesis, *Phys. Rev. D* 56 (1997) 3191–3197. arXiv:astro-ph/9703065, doi:10.1103/PhysRevD.56.3191.
- [38] C. J. Smith, G. M. Fuller, M. S. Smith, Big bang nucleosynthesis with independent neutrino distribution functions, *Phys. Rev. D* 79 (10) (2009) 105001. arXiv:0812.1253, doi:10.1103/PhysRevD.79.105001.
- [39] A. Steyerl, J. M. Pendlebury, C. Kaufman, S. S. Malik, A. M. Desai, Quasielastic scattering in the interaction of ultracold neutrons with a liquid wall and application in a reanalysis of the Mambo I neutron-lifetime experiment, *Phys. Rev. C* 85 (6) (2012) 065503. doi:10.1103/PhysRevC.85.065503.
- [40] A. T. Yue, M. S. Dewey, D. M. Gilliam, G. L. Greene, A. B. Laptev, J. S. Nico, W. M. Snow, F. E. Wietfeldt, Improved Determination of the Neutron Lifetime, *Physical Review Letters* 111 (22) (2013) 222501. arXiv:1309.2623, doi:10.1103/PhysRevLett.111.222501.
- [41] J. Bernstein, L. S. Brown, G. Feinberg, Cosmological helium production simplified, *Reviews of Modern Physics* 61 (1989) 25–39. doi:10.1103/RevModPhys.61.25.

- [42] Y.-Z. Qian, G. M. Fuller, G. J. Mathews, R. W. Mayle, J. R. Wilson, S. E. Woosley, Connection between flavor mixing of cosmologically significant neutrinos and heavy element nucleosynthesis in supernovae, *Physical Review Letters* 71 (1993) 1965–1968. doi:10.1103/PhysRevLett.71.1965.
- [43] P. F. de Salas, S. Pastor, Relic neutrino decoupling with flavour oscillations revisited, *ArXiv e-prints* arXiv:1606.06986.
- [44] K. Abazajian, N. F. Bell, G. M. Fuller, Y. Y. Y. Wong, Cosmological lepton asymmetry, primordial nucleosynthesis and sterile neutrinos, *Phys. Rev. D* 72 (6) (2005) 063004. arXiv:astro-ph/0410175, doi:10.1103/PhysRevD.72.063004.
- [45] G. M. Fuller, C. T. Kishimoto, A. Kusenko, Heavy sterile neutrinos, entropy and relativistic energy production, and the relic neutrino background, *ArXiv e-prints* arXiv:1110.6479.
- [46] J. L. Menestrina, R. J. Scherrer, Dark radiation from particle decays during big bang nucleosynthesis, *Phys. Rev. D* 85 (4) (2012) 047301. arXiv:1111.0605, doi:10.1103/PhysRevD.85.047301.
- [47] H. Ishida, M. Kusakabe, H. Okada, Effects of long-lived 10 MeV-scale sterile neutrinos on primordial elemental abundances and the effective neutrino number, *Phys. Rev. D* 90 (8) (2014) 083519. arXiv:1403.5995, doi:10.1103/PhysRevD.90.083519.
- [48] D. Boyanovsky, Space-time evolution of heavy sterile neutrinos in cascade decays, *Nuclear Physics B* 888 (2014) 248–270. arXiv:1406.5739, doi:10.1016/j.nuclphysb.2014.09.018.
- [49] D. Boyanovsky, Nearly degenerate heavy sterile neutrinos in cascade decay: Mixing and oscillations, *Phys. Rev. D* 90 (10) (2014) 105024. arXiv:1409.4265, doi:10.1103/PhysRevD.90.105024.
- [50] L. Lello, D. Boyanovsky, Cosmological implications of light sterile neutrinos produced after the QCD phase transition, *Phys. Rev. D* 91 (6) (2015) 063502. arXiv:1411.2690, doi:10.1103/PhysRevD.91.063502.
- [51] N. Vassh, E. Grohs, A. B. Balantekin, G. M. Fuller, Majorana neutrino magnetic moment and neutrino decoupling in big bang nucleosynthesis, *Phys. Rev. D* 92 (12) (2015) 125020. arXiv:1510.00428, doi:10.1103/PhysRevD.92.125020.